Gregory V. Nikiforovich[1]
Manfred Mutter[2]
Christian Lehmann[2]
[1] *Center for Molecular Design, Washington University, Box 8036, St. Louis, MO 63110, USA*

[2] *University of Lausanne, BCH-Dorigny, CH-1015 Lausanne, Switzerland*

Molecular Modeling and Design of Regioselectively Addressable Functionalized Templates with Rigidified Three-Dimensional Structures

Abstract: *Extensive conformational analysis of a series of β-alkyl substituted cyclopeptides—* cyclo*(Pro[1]–Xaa[2]–Nle[3]–Ala[4]–Nle[5]–Pro[6]–Xaa[7]–Nle[8]–Ala[9]–Nle[10]) and* cyclo*[Pro[1]–Xaa[2]–Nle[3]–(Cys[4]–Nle[5]–Pro[6]–Xaa[7]–Nle[8]–Cys[9])–Nle[10]] as well as their corresponding unsubstituted core structures* cyclo*(Pro[1]–Xaa[2]–Ala[3]–Ala[4]–Ala[5]–Pro[6]–Xaa[7]–Ala[8]–Ala[9]–Ala[10]) and* cyclo*(Pro[1]–Xaa[2]–Ala[3]–Cys[4]–Ala[5]–Pro[6]–Xaa[7]–Ala[8]–Cys[9]–Ala[10]) has been performed employing both the ECEPP/2 and the MAB force fields (Xaa = Gly, L-Ala, D-Ala, Aib, and D-Pro). Results show that (a) possible three-dimensional structures of the* cyclo*(Pro[1]–Gly[2]–Lys[3]–Ala[4]–Lys[5]–Pro[6]–Gly[7]–Lys[8]–Ala[9]–Lys[10]) molecule are not limited to a single extended "rectangular" conformation with all Lys side chains oriented at the same side of the molecule; (b) conformational equilibrium in monocyclic analogues obtained by replacements of conformationally flexible Gly residues for L-Ala, D-Ala, Aib, or D-Pro is not significantly shifted towards the target "rectangular" conformational type; and (c) introduction of disulfide bridges between positions 4 and 9 is a very powerful way to stabilize the target conformations in the resulting bicyclic molecules. These findings form the basis for further design of rigidified regioselectively addressable functionalized templates with many application areas ranging from biostructural to diagnostic purposes.* © 1999 John Wiley & Sons, Inc. Biopoly 50: 361–372, 1999

Keywords: *conformational analysis; molecular modeling; cyclopeptides; templates*

INTRODUCTION

Protein design aims to mimic some of the structural and functional properties of native proteins.[1–4] The complexity of the folding mechanism, i.e., the pathway by which a linear polypeptide chain finds its unique three-dimensional (3D) structure, represents one of the most intriguing hurdles in this rapidly growing field. In order to bypass this well-known protein-folding problem,[5] some years ago we proposed the construction of non-native chain architectures with a high propensity for folding.[6,7] According

This paper is dedicated to Professor Hans Dahn on the occasion of his 80th birthday.

Correspondence to: G. V. Nikiforovich or Christian Lehmann

Contract grant sponsor: NIH and Swiss National Science Foundation
Contract grant number: 48184 (NIH)
Biopolymers, Vol. 50, 361–372 (1999)

CCC 0006-3525/99/040361-12

to this concept, termed TASP (template-assembled synthetic proteins), topological templates[8,9] are used as a built-in device for directing covalently attached peptide blocks to a predetermined packing arrangement, resulting in branched chain architectures.

The use of templates to direct organic synthesis has a long-standing history. More recently, topological templates have become a versatile tool in peptide mimicry, and their full potential is only now about to be recognized.[10] In view of the expanding areas of applications and functions, topological templates may be generally characterized as synthetic devices, that orient functional groups or structural units in well-defined spatial arrangements. Typically, template molecules represent structural motifs such as constrained peptides, cyclodextrines, or polycyclic systems disposing selectively addressable functional groups. The use of templates exhibiting a predetermined backbone conformation as host for the selective attachment of functional sites (e.g., amino acid side chains or peptides) represents a conceptually new approach in molecular recognition studies and peptides mimicry. These topological templates disposing functional groups in spatially defined positions for interaction with an acceptor molecule are ideal candidates to mimic bioactive conformations for peptide ligands or protein surfaces, e.g., discontinuous epitopes, binding, and catalytic sites. A number of most encouraging applications of this concept have been reported recently.[11–15]

As template molecules, constrained cyclic peptides or stabilized secondary structure elements such as helices, sheets, loops, or turns proved to be versatile structural motifs for disposing selectively addressable groups. Alternative motifs such as cyclodextrins, glycosidic moieties, or polycyclic systems might also be feasible templates for specific applications.

In case of small peptide molecules, most experimental approaches such as CD, ir, nmr, and electron spin resonance deliver the values of measured structural parameters for an average conformation in solution, and it is a separate and nontrivial task to extract information relevant to any particular 3D structure (see, e.g., Ref. 16). The same conformational averaging may prevent crystallization, and consequently, obtaining x-ray data. Molecular modeling, on the other hand, can provide detailed information on each of the low-energy conformers of the molecule. However, this information will critically depend on many factors, e.g., the force field that has been used and the calculation protocols involved (see, e.g., Ref. 17). Accordingly, results of molecular modeling should be carefully validated for consistency with the available experimental data. At the same time, molecular modeling has a very important advantage from the design point of view, since it allows to predict possible 3D structures for various molecules before actual chemical synthesis of individual compounds.

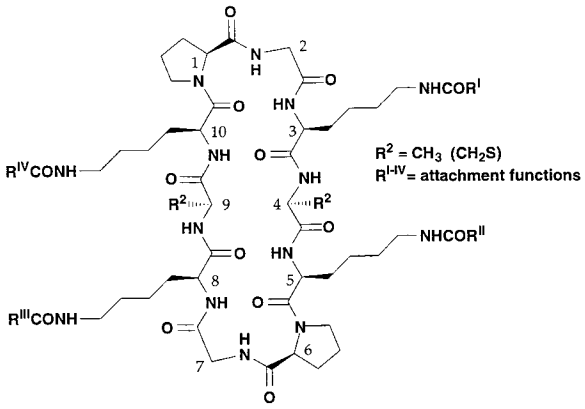

FIGURE 1 Cyclodecapeptides presently studied as the RAFT class of molecules.

So far, experimental studies of 3D structures of template and TASP molecules have been limited to nmr and CD measurements for several cyclic template peptides (RAFT, the regioselectively addressable functionalized templates, cf. Figure 1) and were undertaken to answer questions raised by molecular dynamics studies performed without experimental restrictions.[18] RAFT molecules, which have been spectroscopically investigated, consisted primarily of the *cyclo*(Pro^1–Gly^2–Lys^3–Ala^4–Lys^5–Pro^6–Gly^7–Lys^8–Ala^9–Lys^{10}) decapeptides with various substituents at the ε-amino groups of the lysine residues.[8] One could expect significant conformational flexibility for the cyclodecapeptides, since even much more constrained cyclopentapeptides reveal conformational averaging in solution.[19] However, as a result of molecular dynamics (MD) simulations restrained by multiple interproton distances measured by nmr in DMSO and applied to a single conformation, only one "rectangular" 3D conformational type of the RAFT backbone has been suggested.[8] That structure consisted of two antiparallel β-strands connected by βII-type turns spanned by the Pro–Gly dipeptide unit.[8] In this structure, the possible attachment positions for peptide fragments to form a TASP, i.e., the side chains of all lysine residues, are directed toward the same side of a best plane defined by the RAFT peptide backbone.

This study presents results of molecular modeling applied to investigate possible 3D structures of the *cyclo*(Pro^1–Gly^2–Lys^3–Ala^4–Lys^5–Pro^6–Gly^7–Lys^8–Ala^9–Lys^{10}) RAFT molecule and to design a variety of analogues to stabilize the desired "rectangular" conformation with two β-turns centered at the Pro–

Gly fragments, and with the spatial arrangement of all Lys side chains at the same side of the RAFT backbone plane. The results of molecular modeling are screened against nmr data obtained previously.[8]

METHODS: FORCE FIELDS AND CALCULATION PROTOCOLS

MAB Force Field Studies

Preliminary molecular modeling studies presented in this work have been performed using the MAB force field developed for a broad variety of compounds important for medicinal chemistry.[20,21] In a typical run, 10,000 conformations of the *cyclo*(Pro[1]–Gly[2]–Ala[3]–Ala[4]–Ala[5]–Pro[6]–Gly[7]–Ala[8]–Ala[9]–Ala[10]) molecule have been generated by a stochastic random generation algorithm. Energy calculations for these conformations have been performed within the MAB force field. In a typical run, 56 different conformations have been selected according to the following criteria: (a) all of them possess relative energies, $E - E_{\min} \leq 10$ kcal/mol; (b) each of them is different from all others by its energy difference $\Delta E \leq 0.1$ kcal/mol, by its deviation in all heavy atom torsional angles, RMSA $\leq 6°$; and by its deviation in all heavy atom interatomic distances, RMSD ≤ 0.1 Å. These 56 conformers form a conformational library ranging by 3D shapes from an extended conformer to a concavely folded one (see Figure 3 below). Second, disulfide bridges were introduced in the two selected limiting structures, the conformations minimized in the force field and their resulting energies compared. The limiting conformations were confirmed to occur in a library generated as described above for [Pro[1]–Gly[2]–Ala[3]–(Cys[4]–Ala[5]–Pro[6]–Gly[7]–Ala[8]–Cys[9])–Ala[10]] with the extended and folded conformations as starting geometries.

ECEPP/2 Force Field Studies

More extensive studies have been performed employing the well-established ECEPP/2 force field developed specifically for peptides and proteins.[22,23] Methods for conformational search and energy calculations were the same as have been validated previously for a variety of peptides.[17] Dihedral angles were the only variables in the process of energy minimization, since a rigid valence geometry with planar *trans* peptide bonds was assumed. Both *trans* and *cis* peptide bonds were examined for the Pro[1,6] residues; in these cases the ω-angles also were allowed to rotate. However, only the *trans* peptide bond configuration has been considered for the D-Pro[2,7] residues within the corresponding analogues, which is in accordance with previous energy calculations for the Pro–D-Pro fragment (Ref. 24; Nikiforovich, unpublished). The valence geometry of the Aib residue was derived from the corresponding crystal data[25]; partial atomic charges were calculated by the use of the SYBYL program (the Gasteiger–Hückel method). Aliphatic and aromatic hydrogens were generally included in united atomic centers of the CH_n type; H^{α}-atoms and amide hydrogens were described explicitly. The value of a macroscopic dielectric constant ε was assumed to be 2.0, which is a standard value for the ECEPP force field. However, some calculations with $\varepsilon = 45$ have been performed to mimic the DMSO environment (see below).

The first step of a calculation protocol in the ECEPP force field consisted of energy calculations for the repeating sequence Ac–Ala–Ala–Pro–Gly–Ala–NMe representing the half of backbone for the entire RAFT molecule. All possible combinations of local energetic minima of *E*, *F*, *C*, *A*, and *A** types (according to the commonly accepted notation[26]) for the peptide backbone of each amino acid residue with the L-configuration were considered at this step. For the L-Pro residues, minima of *F*, *C*, and *A* types have been considered, as well as minima of *E*, *F*, *C*, *A*, *A**, *C**, *F**, and *E** types have been considered for the Gly residues. The total number of all low-energy conformers (i.e., those satisfying an energy criterion of $\Delta E = E - E_{\min} = \Delta E \leq 10$ kcal/mol) for the Ac–Ala–Ala–Pro–Gly–Ala–NMe fragment was 1123.

Several filters have subsequently been used to lower the number of conformers for the entire RAFT molecule to be considered at further steps. For instance, it was reasonable to assume that the Ala–Ala–Pro–Gly–Ala pentapeptide being included into a cyclodecapeptide structure will possess only conformers with the distance limitation of 5.0 Å $\leq C_{\alpha(1)}—C_{\alpha(5)} \leq$ 12.0 Å. The total number of such low-energy conformers was 899, which would give $899 \times 899 = 808{,}201$ possibilities for the entire RAFT molecule. However, if the same distance limitation as above is applied for every $C_{\alpha(i)}—C_{\alpha(i+4)}$ distance, 6615 possible conformers of the backbone for the entire RAFT molecule are obtained. Each of these conformers has been subjected to energy calculations independently for the five molecules representing the peptide backbones of the corresponding RAFT analogues. The molecules in question have been as follows:

cyclo(Pro[1]–Gly[2]–Ala[3]–Ala[4]–Ala[5]–Pro–Gly[7]–Ala[8]–Ala[9]–Ala[10]), molecule ***i***;
cyclo(Pro[1]–Ala[2]–Ala[3]–Ala[4]–Ala[5]–Pro[6]–Ala[7]–Ala[8]–Ala[9]–Ala[10]), molecule ***ii***;
cyclo(Pro[1]–D-Ala[2]–Ala[3]–Ala[4]–Ala[5]–Pro[6]–D-Ala[7]–Ala[8]–Ala[9]–Ala[10]), molecule ***iii***;
cyclo(Pro[1]–Aib[2]–Ala[3]–Ala[4]–Ala[5]–Pro[6]–Aib[7]–Ala[8]–Ala[9]–Ala[10]), molecule ***iv***;
cyclo(Pro[1]–D-Pro[2]–Ala[3]–Ala[4]–Ala[5]–Pro[6]–D-Pro[7]–Ala[8]–Ala[9]–Ala[10]), molecule ***v***.

Energy minimization revealed 391 low-energy conformers (the same energy criterion of $\Delta E = 10$ kcal/mol) for molecule ***i***, 205 for molecule ***ii***, 225 for molecule ***iii***, 146 for molecule ***iv***, and 102 for molecule ***v***. For every molecule, each of these conformers differs from others by more than 40° in at least one value of any backbone dihedral angle. At the next step, the Nle residues have been added to the RAFT molecules representing the charged lysine residues. Omission of terminal ε-amino groups allowed to exclude from

conformational energy any unnecessary additional electrostatic interactions that can perturb 3D structures of actually obtained RAFTs where the ε-amino groups of lysins are substituted. The dihedral angle values of the Nle side chains have been optimized before final energy minimization to achieve their most favorable spatial arrangements employing the algorithm described earlier.[27]

Subsequently, energy calculations have been performed starting from the low-energy backbone conformers found previously for the following molecules:

cyclo(Pro[1]–Gly[2]–Nle[3]–Ala[4]–Nle[5]–Pro[6]–Gly[7]–Nle[8]–Ala[9]–Nle[10]), molecule **I**;
cyclo(Pro[1]–Ala[2]–Nle[3]–Ala[4]–Nle[5]–Pro[6]–Ala[7]–Nle[8]–Ala[9]–Nle[10]), molecule **II**;
cyclo(Pro[1]–D-Ala[2]–Nle[3]–Ala[4]–Nle[5]–Pro[6]–D-Ala[7]–Nle[8]–Ala[9]–Nle[10]), molecule **III**;
cyclo(Pro[1]–Aib[2]–Nle[3]–Ala[4]–Nle[5]–Pro[6]–Aib[7]–Nle[8]–Ala[9]–Nle[10]), molecule **IV**;
cyclo(Pro[1]–D-Pro[2]–Nle[3]–Ala[4]–Nle[5]–Pro[6]–D-Pro[7]–Nle[8]–Ala[9]–Nle[10]), molecule **V**.

At this step, energy minimization yielded 174 different low-energy conformers (the same energy criterion) for molecule **I**, 89 for molecule **II**, 94 for molecule **III**, 72 for molecule **IV**, and 47 for molecule **V**. These conformers were regarded as final results, and were used for further analysis of 3D shapes of the RAFT molecules.

The above obtained low-energy backbone conformers were further used as starting points for energy calculations of the bicyclic molecules of the following types:

bicyclo[Pro[1]–Gly[2]–Nle[3]–(Cys[4]–Nle[5]–Pro[6]–Gly[7]–Nle[8]–Cys[9])–Nle[10]], molecule **Is**;
bicyclo[Pro[1]–Ala[2]–Nle[3]–(Cys[4]–Nle[5]–Pro[6]–Ala[7]–Nle[8]–Cys[9])–Nle[10]], molecule **IIs**;
bicyclo[Pro[1]–D-Ala[2]–Nle[3]–(Cys[4]–Nle[5]–Pro[6]–D-Ala[7]–Nle[8]–Cys[9])–Nle[10]], molecule **IIIs**;
bicyclo[Pro[1]–Aib[2]–Nle[3]–(Cys[4]–Nle[5]–Pro[6]–Aib[7]–Nle[8]–Cys[9])–Nle[10]], molecule **IVs**;
bicyclo[Pro[1]–D-Pro[2]–Nle[3]-(Cys[4]–Nle[5]–Pro[6]–D-Pro[7]–Nle[8]–Cys[9])–Nle[10]], molecule **Vs**.

The dihedral angle values of the Cys side chains (as well as the Nle's side chains) were optimized before final energy minimization to achieve their most favorable spatial arrangements employing the algorithm described earlier.[27] Finally, energy calculations have revealed significantly reduced conformational possibilities for the bicycles compared to the monocyclic RAFT molecules. Namely, there have been found 8 low-energy conformers (the same energy criterion) for molecule **Is**, 1 for molecule **IIs**, 4 for molecule **IIIs**, 3 for molecule **IVs**, and 14 for molecule **Vs**.

RESULTS AND DISCUSSION

RAFT Low-Energy Conformations in DMSO

As was mentioned above, results of molecular modeling need to be confronted with available experimental data. The available data for the *cyclo*(Pro[1]-Gly[2]–Lys[3]–Ala[4]–Lys[5]–Pro[6]–Gly[7]–Lys[8]–Ala[9]–Lys[10]) RAFT molecule include nmr measurements in DMSO.[8] Since the most rigorous and reliable data obtainable by nmr spectroscopy are interproton distances deduced from the nuclear Overhauser effect (NOE) measurements,[28] we have chosen for comparison with calculated 3D structures the 28 different interproton distances between α-protons, amide-protons, and δ-protons of Pro residues deduced from NOEs measured in DMSO (Table IV in Ref. 8). The distances are listed in the last column of Table I.

Experimental interproton distances listed in Table I cannot be consistently satisfied by one single conformation. For instance, Ref. 8 lists three interdependent distances, namely $\alpha H_{Ala4/9}$—$NH_{Ala4/9}$ = 2.89/2.89 Å; $\alpha H_{Ala4/9}$—$NH_{Lys5/10}$ = 2.23/2.38 Å; and $NH_{Ala4/9}$—$NH_{Lys5/10}$ = 2.17/2.47 Å. If the first two distances are valid, the values of backbone dihedral angles for Ala[4/9] should be ca. $\phi = -120°$, $\psi = 120°$. In this case, the third distance is over 4.0 Å (see Figure 2), which would produce a much less intense NOE than observed and calibrated to an interproton distance of 2.2–2.5 Å. Otherwise, significant distortions of the valence geometry of the Ala[4/9] residues are required, which does not seem likely in a relatively nonconstrained cyclic decapeptide.

The above considerations question a single 3D structure of RAFT satisfying all measured nmr parameters, as has been proposed earlier.[8] Indeed, the restrained MD simulations that have been applied to the RAFT molecule have employed the consistent valence force field (CVFF) known to tolerate significant distortions of valence angles.[29] Most importantly, the $NH_{Lys3/5}$—$O_{Lys10/8}$ and $N_{Lys3/5}$—$O_{Lys10/8}$ distances characteristic for transannular hydrogen bonds of the $Lys_{3/8}NH \cdots OCLys_{10/5}$ and $Lys_{5/10}NH \cdots OCLys_{8/3}$ types have also been included in the previous MD simulations as restrictions (Ref. 8, Table IV), despite these distances cannot be reliably determined by nmr measurements. The latter are in fact only indirectly determined and inferred from temperature-dependent shift gradients in the nmr spectrum, an effect that goes back to an observation exploited at pioneering times of nmr spectroscopy.[30,31] It is legitimate to conclude, then, that the single RAFT conformer deduced earlier may present a too simplified view on a much more complex conformational equilibrium existing in DMSO solution.

The preliminary studies performed with the MAB force field offered extreme boundaries for a conformational equilibrium that may be more likely to occur than one single conformer. The calculations that sampled space without any a priori constraints other than the initial *cis*/*trans* and chiral constraints yielded a

Table I Experimentally Measured Interproton Distances Compared to Their Values in Two Limiting Conformers Obtained by MAB Force Field, and to Upper and Lower Limits Calculated for 136 Low-Energy Conformers Obtained by ECEPP Force Field (Å)

	MAB		ECEPP/2 Calculated Values		
Distance	Extended	Folded	Lower	Upper	NMR Measured Values[8]
$Pro^{1}H\delta^{pro\text{-}R}$—$Lys^{10}H\alpha$	2.03	2.31	2.02	2.42	2.23
$Pro^{1}H\delta^{pro\text{-}S}$—$Lys^{10}H\alpha$	2.85	2.47	2.31	2.79	2.29
$Gly^{2}H\alpha^{pro\text{-}R}$—$Gly^{2}NH$	2.67	2.51	2.35	2.90	2.22
$Gly^{2}H\alpha^{pro\text{-}S}$—$Gly^{2}NH$	3.07	3.08	2.34	2.92	2.80
$Gly^{2}H\alpha^{pro\text{-}R}$—$Lys^{3}NH$	3.59	3.44	2.82	3.64	2.88
$Gly^{2}H\alpha^{pro\text{-}S}$—$Lys^{3}NH$	3.01	3.36	2.60	3.49	2.81
$Gly^{2}NH$—$Lys^{3}NH$	2.33	2.23	2.28	3.92	2.73
$Pro^{1}H\alpha$—$Gly^{2}NH$	2.16	2.22	2.22	3.37	2.33
$Lys^{3}H\alpha$—$Lys^{3}NH$	3.01	3.08	2.43	2.98	2.89
$Ala^{4}H\alpha$—$Lys^{5}NH$	2.24	**3.70**	2.33	3.34	2.23
$Ala^{4}H\alpha$—$Ala^{4}NH$	3.08	3.06	2.33	2.96	2.89
$Lys^{3}H\alpha$—$Ala^{4}NH$	2.29	**3.66**	2.41	3.50	2.07
$Ala^{4}NH$—$Lys^{5}NH$	**4.14**	2.25	2.37	3.95	2.17
$Lys^{5}H\alpha$—$Lys^{5}NH$	3.07	3.07	2.60	3.03	2.89
$Pro^{6}H\delta^{pro\text{-}R}$—$Lys^{5}H\alpha$	2.03	2.37	1.94	2.57	2.23
$Pro^{6}H\delta^{pro\text{-}S}$—$Lys^{5}H\alpha$	2.85	3.04	2.19	2.85	2.29
$Gly^{7}H\alpha^{pro\text{-}R}$—$Gly^{7}NH$	2.67	2.51	2.37	2.91	2.22
$Gly^{7}H\alpha^{pro\text{-}S}$—$Gly^{7}NH$	3.07	3.08	2.38	2.93	2.82
$Gly^{7}H\alpha^{pro\text{-}R}$—$Lys^{8}NH$	3.59	3.44	2.84	3.70	2.88
$Gly^{7}H\alpha^{pro\text{-}S}$—$Lys^{8}NH$	3.01	3.36	2.53	3.42	2.81
$Gly^{7}NH$—$Lys^{8}NH$	2.33	2.23	2.26	3.82	2.82
$Pro^{6}H\alpha$—$Gly^{7}NH$	2.16	2.22	2.17	3.32	2.30
$Lys^{8}H\alpha$—$Lys^{8}NH$	3.01	3.08	2.65	2.98	2.89
$Ala^{9}H\alpha$—$Lys^{10}NH$	2.24	**3.70**	2.24	3.17	2.38
$Ala^{9}H\alpha$—$Ala^{9}NH$	3.08	3.06	2.43	2.99	2.89
$Lys^{8}H\alpha$—$Ala^{9}NH$	2.29	**3.66**	2.27	3.41	2.24
$Ala^{9}NH$—$Lys^{10}NH$	**4.14**	2.25	2.60	4.20	2.47
$Lys^{10}H\alpha$—$Lys^{10}NH$	3.07	3.07	2.55	3.03	2.89

conformational library ranging from the "extended" conformer to the "folded" one (Figure 3). In the presently applied force field, the extended conformer, which corresponds to the target RAFT structure, possesses a conformational energy which is more than 8 kcal/mole higher than the energy of the concavely folded conformer; this is in contrast to the CVFF and the ECEPP force fields, which locate the extended conformer below the folded one.[18] In the latter, the βII-type turn geometry of the Pro–Gly turn is fully conserved, with a tendency to bifurcated hydrogen bonding to the proline CO group in the cavity. It should be noted that both conformers have the hydrogens along the three central NH—CαH bonds oriented antiperiplanar and are therefore consistent with dihedral angle constraints derived from an intraresidual coupling constant $^{3}J_{\alpha NH} > 8$ Hz (cf., e.g., Ref. 28, p. 167). In the folded low-energy conformation, all of the hydrogen bonds point to the interior of the molecule, and therefore a correspondingly strong shielding can easily be accounted for.

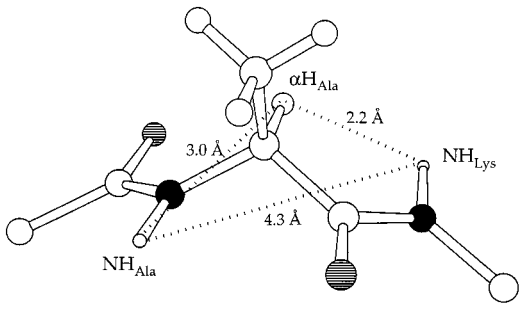

FIGURE 2 Interproton distances corresponding to $\phi = -120°$, $\psi = 120°$ with standard valence geometry.

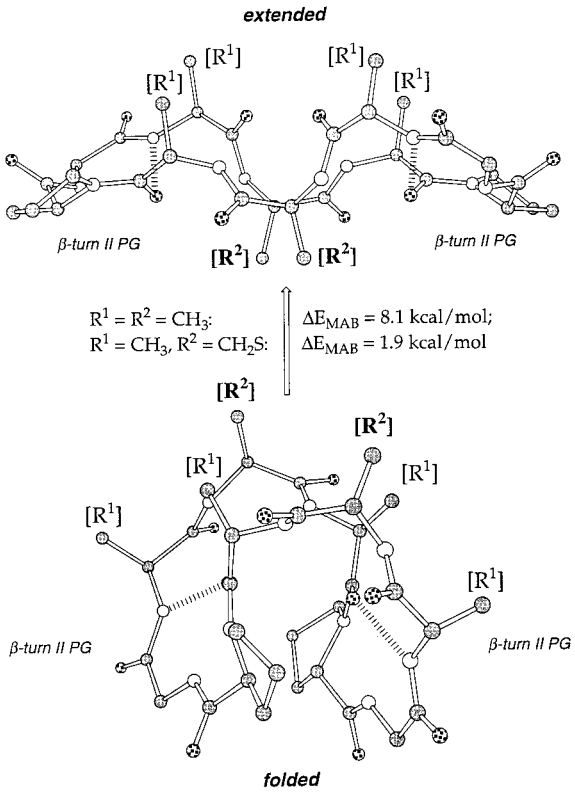

FIGURE 3 Rectangular "extended" conformer of the template core (top) together with a concavely "folded" low-energy conformer (bottom).

These two conformers are the "limiting" ones in the obtained conformational library, and neither of them satisfies all experimental distances to the degree of a well-balanced calibration (see the second and third column of Table I). It is evident from the comparison of the distances in the limiting structures, that the folded conformer relieves a distance violation above 4 Å ($NH_{Ala4/9}$—$NH_{Lys5/10}$; cf. Table I) occurring in the extended conformer in favor of two distances $\alpha H_{Ala4/9}$—$NH_{Lys5/10}$ and $\alpha H_{lys3/8}$—$NH_{Ala4/9}$ below 4 Å in the folded one, and therefore agrees slightly better with the particular experimental values (see entries printed bold in Table I). Since this conformational averaging leaves the φ-angle unchanged as pointed out above ($^3J_{\alpha NH}$), we may term it "ψ-rocking" (cf. Figure 4).

This oscillation can occur over a considerable range of ψ values, covering a vertical sector ($\varphi = -120 \pm 30°$; $\theta = -180° \pm 30°$, cf. Ref. 28, p. 167) within the Ramachandran map over the regions denoted as β_E and α_R[32] with ψ-angles from $+120°$ to $-60°$, respectively. Thereby in the present case the measured $\alpha H_{Ala4/9}$—$NH_{Lys5/10}$ distances (2.23/2.38 Å) conform with the extended β-region, whereas the measured $NH_{Ala4/9}$—$NH_{Lys5/10}$ distances (2.17/2.47 Å) conform with the α-region. However, the ψ-rocking cannot account for experimental values of all three distances in question simultaneously, namely $\alpha H_{Ala4/9}$—$NH_{Ala4/9}$ = 2.89/2.89 Å; $\alpha H_{Ala4/9}$—$NH_{Lys5/10}$ = 2.23/2.38 Å; and $NH_{Ala4/9}$—$NH_{Lys5/10}$ = 2.17/2.47 Å in one single conformer.

To compare calculations employing the ECEPP force field with nmr data, we have performed the additional energy calculations for the *cyclo*(Pro^1–Gly^2–Lys^3–Ala^4–Lys^5–Pro^6–Gly^7–Lys^8–Ala^9–Lys^{10}) RAFT molecule with $\varepsilon = 45$ mimicking to some extent DMSO environment. These calculations have employed 391 low-energy backbone conformers as starting points, and have yielded 136 low-energy conformers ($\Delta E = 10$ kcal/mol) for the RAFT molecule to be compared with experimental data. Again, none of these conformers alone satisfies all of the experimental interproton distances listed in the last column of Table I.

Conformational averaging can be treated in a statistical way by the approach developed by us previously.[16,33] It suggests that experimentally measured and calculated conformational parameters are in good agreement when their mean values are statistically indistinguishable. In other words, for each conformational parameter A, the following condition between the experimental value $\langle A^{exp} \rangle$ and the weighted sum of calculated values $\langle A^{calc} \rangle$ should be satisfied:

$$\frac{|\sum_{i=1}^{N} w_i \langle A^{calc} \rangle_{ik} - \langle A^{exp} \rangle_k|}{\sum_{i=1}^{N} (w_i D_{ik}^{calc})^2 + (D_k^{exp})^2]^{1/2}} < \mathbf{t}_k$$

Here i and k are indexes related to the number of low-energy conformers (N) and to the number of

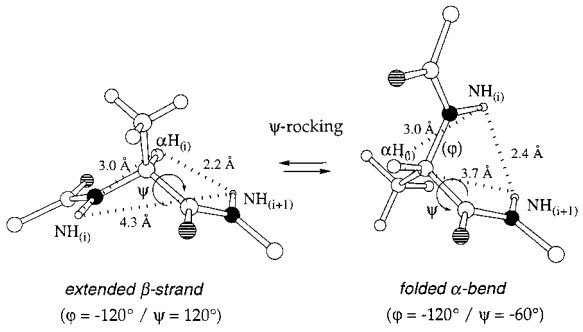

FIGURE 4 Oscillation around the angle ψ ("ψ-rocking") generates limiting local peptide backbone conformations conserving the ϕ-angle value.

measured parameters (M), respectively, whereas **t** is the Student's coefficient at the chosen confidence level; the w_i are statistical weights of low-energy conformers; and the D are standard deviations of mean values for the calculated and experimentally measured parameters. Estimation of statistical weight values w_i can be performed by random generation of the K N-dimensional $\{w_i\}$ points, each point satisfying all M above inequalities as well as conditions of $w_i = 0$, and $\Sigma_i^N w_i = 1$. Each point of the ensemble represents the possible statistical weights for all N conformers compatible with the available experimental data. Averaging over the ensemble would produce the mean values $\langle w_i \rangle$ and their standard deviations SD_i for the statistical weights estimated for each of the low-energy conformers, as well as their upper and lower limits w_i^{up} and w_i^{low}.

The above approach is not limited by a number of low-energy conformers, and, generally speaking, it might be applied to our case with $N = 136$ and $M = 28$, as well. However, it should be expected that the values of statistical weights spread over 136 conformers would be rather low, hardly reaching 0.01. On the other side, the reliability of estimates for the $\langle w_i \rangle$ values would require an enormous number of randomly generated $\{w_i\}$ points (e.g., for $N = 14$, K has been well over 500,000, Ref. 16). It is noteworthy also that an accuracy of our energy estimations is limited by neglecting effects of solvation. For these reasons, it seems reasonable to assume, as a first approximation, that all 136 conformers would have the same mean statistical weight values in DMSO. Table I lists the upper and lower limits ($\langle A \rangle \pm$ SD) for each of the 28 experimentally measured interproton distances averaged over all 136 conformers (the fourth and fifth columns, respectively). Only in 8 cases out of 28, the experimental values are out of this range for calculated distances. The maximal deviation out of this range is 0.34 Å (for the NH_{Ala4}—αH_{Lys3} distance), and the average deviation over 8 distances is 0.14 Å, which is well inside the errors of both measurements and calculations. Therefore, it can be stated that averaging over all 136 low-energy RAFT conformers obtained by energy calculations easily reproduce available experimental data even in the simplest assumption that their statistical weight values are equal. In turn, that validates the employed methods and protocols of energy calculations.

RAFT Low-Energy Conformations and Design of Rigidified RAFT Molecules

The "target" 3D structure for the particular type of the *cyclo*(Pro^1–Gly^2–Lys^3–Ala^4–Lys^5–Pro^6–Gly^7–Lys^8–Ala^9–Lys^{10}) RAFT molecule is the extended "rectangular" conformation with two β-turns centered at the Pro–Gly fragments, and with the spatial arrangement of all Lys side chains "at the same side" of the RAFT backbone plane normal to the attachment vectors. Energy calculations employing the standard ECEPP/2 force field (i.e., with $\varepsilon = 2.0$) revealed that this molecule is of significant conformational flexibility possessing 174 different low-energy conformers of the backbone. Of course, not all of them correspond to the target 3D structure. Conformers similar to the 3D structure in question can be selected according to the obvious geometrical limitations. First, both suggested β-turns should satisfy definitions of the β-turn, i.e., distances C_{10}^{α}—C_3^{α} and C_5^{α}—C_8^{α} should be less than 7 Å.[33] The same limitation could be required for the C_4^{α}—C_9^{α} distance, which would ensure the β-sheet-like structure of the cyclodecapeptide. At the same time, amino acid residues constituting the opposite β-turns should be rather far from each other, which suggests the following limitations: C_1^{α}—C_7^{α}, C_1^{α}—C_6^{α}, C_2^{α}—C_6^{α} and C_2^{α}—$C_7^{\alpha} > 12$ Å. As to the spatial arrangement of all Lys (Nle) side chains "at the same side" of the backbone plane, it can be verified by fulfillment of requirement that the absolute value of angles between vectors C_i^{α}—C_j^{ε} for all Lys's (Nle's) is less than 60° ($i \neq j = 3$, 5, 8, and 10).

The above limitations have been applied to the 174 low-energy RAFT conformers. It appeared that 28 of them are compatible to the limitations, and therefore, can be regarded as similar to the target 3D structure. It consists about 16% of all low-energy structures. All selected conformers contain only *trans* peptide bond for both Pro residues. Also, in all cases, the $Nle^{5/10}$ residues preceding prolines possess the negative ϕ and positive ψ values. The positive ψ values are characteristic also for both $Ala^{4/9}$ residues; however, the ϕ values for them can be either positive or negative. The 28 conformers represent various types of the Pro–Gly β-turns. The most populated one is the type resembling the βII-turn (see conformer **a** in Table II), or that almost exactly reproducing the βII-turn (see conformer **b** in Table II). In combinations, both these turn types produce symmetrical 3D structures with intrabackbone hydrogen bonds either of the Gly_2/$Ala_4NH \cdots OCNle_{10}$ and Gly_7/$Ala_9NH \cdots OCNle_8$ types (conformer **a** in Figure 5), or of the $Nle_{3/8}$ $NH \cdots OCNle_{10/5}$ and $Nle_{10/5}NH \cdots OCNle_{3/8}$ types (conformer **b** in Figure 5). Less populated are the turn types similar to the βIII-turn (the Pro^1–Gly^2 sequence in conformer **c**, Table II), or the βI-turn (the Pro^6–Gly^7 sequence in conformer **c**, Table II). These turns do not form symmetrical 3D structures; their combination is depicted in Figure 5 (conformer **c**) as an example. Note that conformer **c**, not being symmetri-

Table II Backbone Dihedral Angles of Typical Low-Energy "Rectangular" Conformers of *cyclo*(Pro[1]–Gly[2]–Nle[3]–Ala[4]–Nle[5]–Pro[6]–Gly[7]–Nle[8]–Ala[9]–Nle[10]) and *bicyclo*[Pro[1]–Gly[2]–Nle[3]–(Cys[4]–Nle[5]–Pro[6]–Gly[7]–Nle[8]–Cys[9])-Nle[10]] Depicted in Figure 5

		Conformers in Figure 5				
Residue	Angle	a)	b)	c)	d)	e)
	ω	172	166	173	168	167
Pro^1	ϕ	−75	−75	−75	−75	−75
	ψ	74	108	−30	74	74
Gly^2	ϕ	158	103	−85	159	162
	ψ	−42	−3	−24	−41	−40
Nle^3	ϕ	−93	−154	−138	−152	−154
	ψ	−43	87	99	132	134
Ala^4/Cys^4	ϕ	50	−96	−79	−98	−92
	ψ	47	110	76	126	140
Nle^5	ϕ	−87	−135	−128	−113	−134
	ψ	157	166	159	165	167
	ω	173	166	−178	169	178
Pro^6	ϕ	−75	−75	−75	−75	−75
	ψ	73	107	−16	85	−16
Gly^7	ϕ	158	101	−112	146	−96
	ψ	−43	0	20	−34	−50
Nle^8	ϕ	−92	−155	−137	−158	−159
	ψ	−43	87	−54	132	126
Ala^9/Cys^9	ϕ	50	−95	57	−110	−85
	ψ	47	108	46	121	131
Nle^{10}	ϕ	−87	−134	−116	−103	−111
	ψ	157	165	163	163	167

cal, still satisfies the main requirements for the target RAFT structure, since all Nle side chains are located at the same side of the slightly twisted "rectangular" backbone plane.

Obvious goals for the design of the rigidified RAFT analogues would be to stabilize the target 3D structure described above, i.e., to increase the percentage of the conformers similar to the target one among the entire variety of low-energy conformers for a given RAFT analogue. In this respect, one can consider several possibilities. First, since the side chains of the $Ala^{4/9}$ residues are close in the target conformation and are directed to the backbone plane side opposite to that featuring the functionally important Lys (Nle) side chains, the corresponding positions could be connected by a valence link, e.g., by substituting the Ala residues for Cys's, which will create a bicyclic molecule. Second, the conformationally flexible $Gly^{2/7}$ residues which are involved in β-turn formation could be replaced by residues with limited conformational possibilities, such as L-Ala (sterically forbidden combinations of positive ϕ and negative ψ values), D-Ala (sterically forbidden combinations of negative ϕ and positive ψ values), Aib (sterically forbidden combinations of the ϕ and ψ values with alternating signs), or D-Pro (the Pro–D-Pro fragment is known as a powerful β-reversal promoter[24,35]). Third, one can use any combination of both kinds of amino acid substitutions.

Energy calculations revealed only 8 low-energy conformers for the *bicyclo*[Pro^1–Gly^2–Nle^3–(Cys^4–Nle^5–Pro^6–Gly^7–Nle^8–Cys^9)–Nle^{10}] molecule (**Is**), and all of them are similar to the target 3D structure. These 8 conformers contain only two types of the Pro–Gly β-turns. The most populated is the one resembling the βII-turn (see Pro–Gly sequence in conformer **d**, Table II), which can form, in combination, symmetrical 3D structures with intrabackbone hydrogen bonds of the $Gly_2/Ala_4NH \cdots OCNle_{10}$ and $Gly_7/Ala_9NH \cdots OCNle_8$ types as well as of the $Nle_{3/8}NH \cdots OCNle_{10/5}$ and $Nle_{10/5}NH \cdots OCNle_{3/8}$ types (conformer **d** in Figure 5). The second turn type is similar to the βIII-turn (the Pro^6–Gly^7 sequence in conformer **e**, Table II). The latter type of β-turn does not form symmetrical 3D structures; the combination of both turns is depicted in Figure 5 (conformer **e**) as an example. Interestingly, the energy gap of ca. 8 kcal/mol obtained between the desired extended β-strand struc-

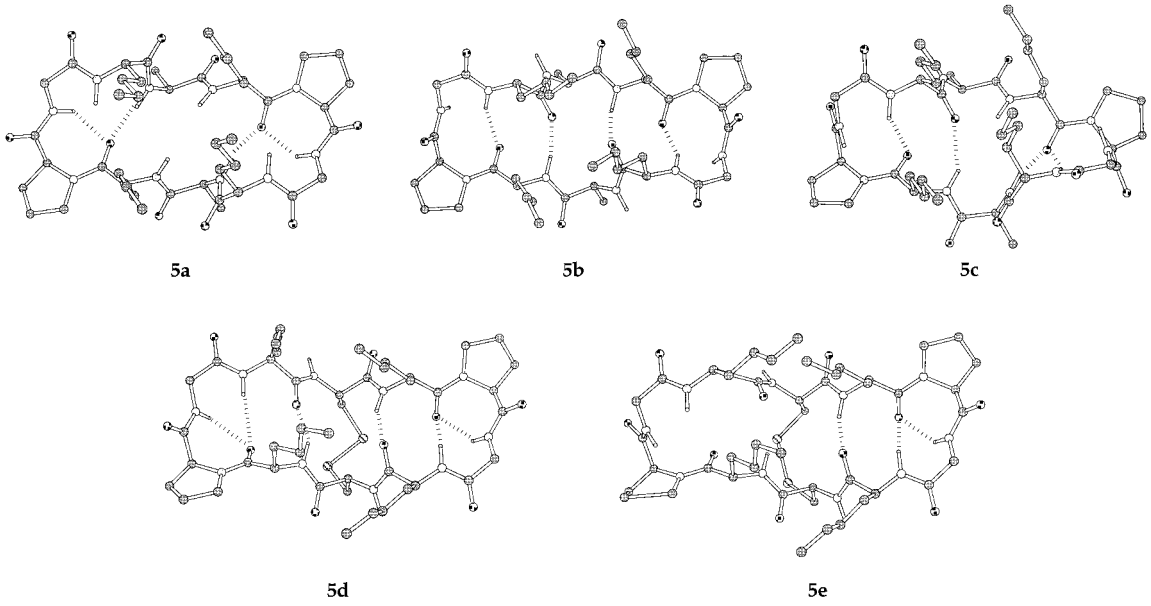

FIGURE 5 Target-like low-energy conformations of *cyclo*(Pro[1]–Gly[2]–Lys[3]–Ala[4]–Lys[5]–Pro[6]–Gly[7]–Lys[8]–Ala[9]–Lys[10]) (conformers **5a** and **5b** are symmetrical ones, conformer **5c** is a nonsymmetrical one) and *bicyclo*[Pro[1]–Gly[2]–Ala[3]–(Cys[4]–Ala[5]-Pro[6]–Gly[7]–Ala[8]–Cys[9])–Ala[10]] (conformer **5d** is a symmetrical one, conformer **5e** is a nonsymmetrical one). All hydrogens except those participating in hydrogen bonds are omitted for clarity. Hydrogen bonds are shown in dashed lines.

ture and the previously obtained concavely folded conformer by employing the MAB force field (see above) was reduced by more than 6 kcal/mole in calculations performed for the *bicyclo*[Pro[1]–Gly[2]–Ala[3]–(Cys[4]–Ala[5]–Pro[6]–Gly[7]–Ala[8]–Cys[9])–Ala[10]] molecule (cf. Figure 3). An energy term analysis shows that repulsive van der Waals interactions forced in the constrained folded geometry by the disulfide bridge most probably play a crucial role in raising its energy.

Whereas connection of positions 4 and 9 by an additional valence link seems to be a very powerful tool to stabilize the target conformation, substitutions of Gly[2/7] by conformationally restricted residues showed much less impressive results. Selection of low-energy conformers similar to the target 3D structure yielded 5 conformations out of 89 (6%) for *cyclo*(Pro[1]–Ala[2]–Nle[3]–Ala[4]–Nle[5]–Pro[6]–Ala[7]–Nle[8]–Ala[9]–Nle[10]); 15 conformations out of 94 (16%) for *cyclo*(Pro[1]–D-Ala[2]–Nle[3]–Ala[4]–Nle[5]–Pro[6]–D-Ala[7]–Nle[8]–Ala[9]–Nle[10]); 8 conformations out of 72 (11%) for *cyclo*(Pro[1]–Aib[2]–Nle[3]–Ala[4]–Nle[5]–Pro[6]–Aib[7]–Nle[8]–Ala[9]–Nle[10]); and 6 conformations out of 47 (13%) for *cyclo*(Pro[1]–D-Pro[2]–Nle[3]–Ala[4]–Nle[5]–Pro[6]–D-Pro[7]–Nle[8]–Ala[9]–Nle[10]). In fact, the target conformation was not stabilized in these analogues compared with the original RAFT molecule (16%, as has been shown above).

It is noteworthy that recent experimental studies of peptides containing sequences D-Pro–X (X = Gly, L-Ala, and D-Ala), which form the "mirror images" of the β-turns spanned by the Pro–X sequences,[36] also did not find any preferences for the D-Pro–L-Ala or D-Pro–D-Ala sequences over D-Pro–Gly as to promotion of β-hairpin structures.[37] Those studies employed nmr spectroscopy in water and did not apply systematic conformational sampling techniques. Our calculations did not involve the D-Pro–X sequences; however, it is could be expected that the "mirror images" of β-turns follow the same or very similar "stabilization patterns" as the β-turns studied above; the very recent experimental work applying the D-Pro–L-Pro template delivers supporting evidence to this suggestion.[38] Nevertheless, we are going to extend our systematic calculations to the "mirror images" of β-turns (in preparation). In particular, we are going to apply our approach to the classic example of gramicidin S, *cyclo*(Pro[1]–Val[2]–Orn[3]–Leu[4]–D-Phe[5]–Pro[6]–Val[7]–Orn[8]–Leu[9]–D-Phe[10]). It is commonly accepted that this peptide possesses a well-defined solution conformation with two symmetrical βII′-turns involving the D-Phe–Pro fragments. The similar conformation has been found by the recent x-ray studies[39]; it features the side chains of the Orn residues on the one side of the β-hairpin plane, and the side chains of the hydrophobic Val and Leu residues on the other side. It could be expected that strong interactions between these hydrophobic side chains (the so-called hydrophobic collapse) would stabilize mirror images of the symmetric

Table III Backbone Dihedral Angles of Typical Low-Energy "Rectangular" Conformers of *cyclo*(Pro[1]–X[2]–Nle[3]–Ala[4]–Nle[5]–Pro[6]–X[7]–Nle[8]–Ala[9]–Nle[10]) and *bicyclo*[Pro[1]–X[2]–Nle[3]–(Cys[4]–Nle[5]–Pro[6]–X[7]–Nle[8]–Cys[9])–Nle[10]] Depicted in Figure 6 (X = L-Ala, D-Ala, Aib, D-Pro)

		Molecules/Conformers in Figure 6							
Residue	Angle	II/a	IIs/a	III/b	IIIs/b	IV/c	IVs/c	V/d	Vs/d
	ω	174	179	172	174	177	172	160	168
Pro[1]	ϕ	−75	−75	−75	−75	−75	−75	−75	−75
	ψ	−22	−19	76	86	147	−46	144	153
X[2]	ϕ	−84	−92	143	142	57	−62	75	75
	ψ	−28	−33	−32	−34	27	−35	−68	−68
Nle[3]	ϕ	−161	−162	−126	−151	−145	−165	−87	−117
	ψ	124	129	91	107	−55	121	76	107
Ala[4]/Cys[4]	ϕ	−89	−76	−82	−79	55	−73	−80	−81
	ψ	84	83	81	103	43	88	74	85
Nle[5]	ϕ	−101	−79	−88	−91	−87	−82	−104	−72
	ψ	163	161	159	159	160	172	163	164
	ω	174	172	172	170	178	171	160	168
Pro[6]	ϕ	−75	−75	−75	−75	−75	−75	−75	−75
	ψ	−22	−29	75	89	147	−45	144	153
X[7]	ϕ	−84	−85	143	143	57	−62	75	75
	ψ	−28	−35	−32	−34	28	−36	−68	−68
Nle[8]	ϕ	−161	−158	−126	−155	−145	−165	−88	−117
	ψ	124	130	91	100	−55	121	76	107
Ala[9]/Cys[9]	ϕ	−90	−73	−83	−82	55	−74	−80	−81
	ψ	84	102	81	101	44	88	75	86
Nle[10]	ϕ	−101	−91	−88	−88	−88	−80	−104	−72
	ψ	163	168	159	157	160	171	163	164

conformations as those of **5b** in Figure 5. However, even the conformation found in crystal is not exactly symmetrical (e.g., one of the Orn residues is involved into intramolecular hydrogen bonding, whereas the other one is not), which might suggest the presence of several possible interconverting conformers for gramicidin S in solution.

Despite the individual substitutions in the Pro–X sequence are not really potent in stabilization of the target RAFT structure, they are instrumental in shifting conformational equilibrium in the target-like conformations towards the particular types of β-turns. Predominant β-turns for *cyclo*(Pro[1]–Ala[2]–Nle[3]–Ala[4]–Nle[5]–Pro[6]–Ala[7]–Nle[8]–Ala[9]–Nle[10]) are those of βIII type; they can form symmetrical structures described in Table III (molecule **II**) and depicted in Figure 6 (conformer **a**). This type of structures contains intrabackbone hydrogen bonds of the $Nle_{3/8}NH \cdots OCNle_{10/5}$ and $Nle_{10/5}NH \cdots OCNle_{3/8}$ types. In the case of *cyclo*(Pro[1]–D-Ala[2]–Nle[3]–Ala[4]–Nle[5]–Pro[6]–D-Ala[7]–Nle[8]–Ala[9]–Nle[10]), the predominant β-turns are those close both to βII and βV types; the corresponding symmetrical structures (Table III, molecule **III**, and Figure 6, conformer **b**) contain the same hydrogen bonds plus two others, namely D-$Ala_2NH \cdots OCPro_1$ and D-$Ala_7NH \cdots OCPro_6$. The predominant β-reversal for symmetrical conformers of *cyclo*(Pro[1]–Aib[2]–Nle[3]–Ala[4]–Nle[5]–Pro[6]–Aib[7]–Nle[8]–Ala[9]–Nle[10]) is not similar to any of the "classical" β-turns (Table III, molecule **IV**, and Figure 6, conformer **c**). These structures contain only two intrabackbone hydrogen bonds, namely $Ala_{4/7}NH \cdots OCPro_{1/6}$. And, finally, the predominant β-turns for *cyclo*(Pro[1]–D-Pro[2]–Nle[3]–Ala[4]–Nle[5]–Pro[6]–D-Pro[7]–Nle[8]–Ala[9]–Nle[10]) are those "between" βII- and βV-turns (Table III, molecule **V**, Figure 6, conformer **d**). The corresponding symmetrical structures, apart from the "crossbackbone" hydrogen bonds $Nle_{10/5}NH \cdots OCD–Pro_{2/6}$ and $Nle_{3/8}NH \cdots OCNle_{10/5}$, contain two "extrabackbone" hydrogen bonds $Ala_{4/9}NH \cdots OCPro_{1/6}$.

The additional disulfide bond between Cys[4] and Cys[9] drastically enhances the ratio of the target-like conformers to the entire number of low-energy conformers of the bicyclic molecules with simultaneous replacements of the Gly[2/7] residues. This ratio is 100% (1 out of 1) for *bicyclo*[Pro[1]–Ala[2]–Nle[3]–(Cys[4]–Nle[5]–Pro[6]–Ala[7]–Nle[8]–Cys[9])-Nle[10]] (Table III, molecule **IIs**; Figure 6, conformer **a**); 100% (**4** out of **4**) for *bicyclo*-

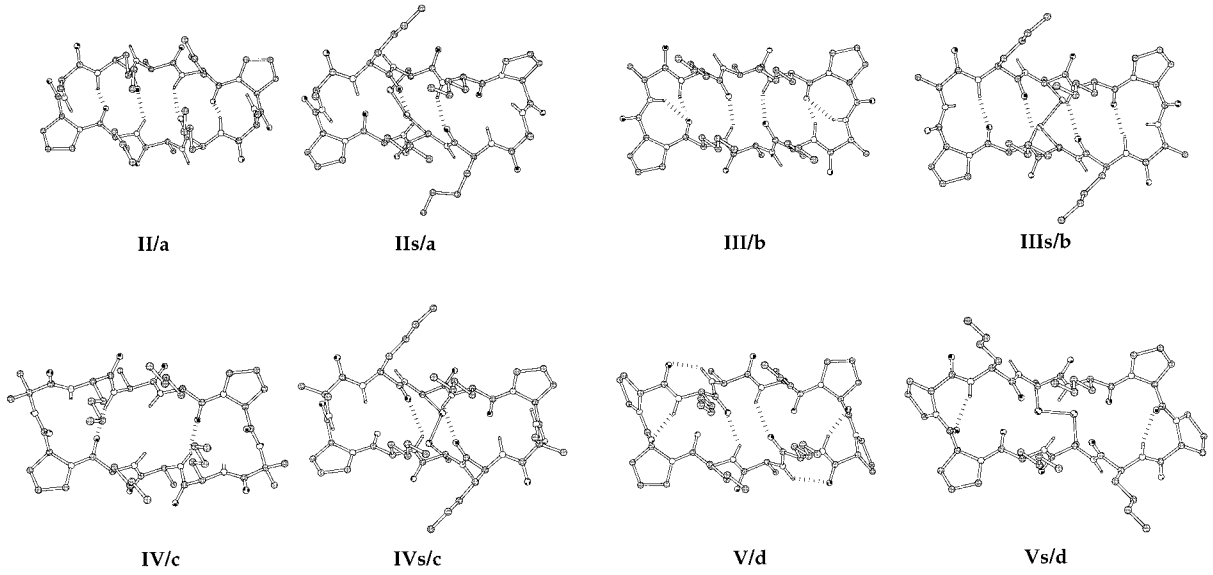

FIGURE 6 Target-like low-energy conformations of Pro–Xaa spanned cyclic decapeptides. The β-turn stabilizing moieties are Pro–L-Ala (**IIa**), Pro–D-Ala (**IIIb**), Pro–Aib (**IVc**), and Pro–D-Pro (**Vd**), respectively. All hydrogens except those participating in hydrogen bonds are omitted for clarity. Hydrogen bonds are shown in dashed lines.

[Pro^1–D-Ala^2–Nle^3–(Cys^4–Nle^5–Pro^6–D-Ala^7–Nle^8–Cys^9)–Nle^{10}] (Table III, molecule **IIIs**; Figure 6, conformer **b**); 67% (2 out of 3) for *bicyclo*[Pro^1–Aib^2–Nle^3–(Cys^4–Nle^5–Pro^6–Aib^7–Nle^8–Cys^9)–Nle^{10}] (Table III, molecule **IVs**; Figure 6, conformer c); and 57% (8 out of 14) for *bicyclo*[Pro^1–D-Pro^2–Nle^3–(Cys^4–Nle^5–Pro^6–D-Pro^7–Nle^8–Cys^9)–Nle^{10}] (Table III, molecule **Vs**; Figure 6, conformer **d**). Interestingly, the systems of intrabackbone hydrogen bonds are somewhat different in the bicyclic molecules compared to corresponding monocycles (see Figure 6). Evidently, it is a consequence of introducing the additional valence link which is much more stable than hydrogen bonds.

CONCLUSIONS

This study demonstrates the applicability of extensive molecular modeling as a tool for rational design of RAFT molecules. The main findings of this study are as follows:

1. Calculations performed with both MAB and ECEPP force fields showed that possible 3D structures of the *cyclo*(Pro^1–Gly^2–Lys^3–Ala^4–Lys^5–Pro^6–Gly^7–Lys^8–Ala^9–Lys^{10}) RAFT molecule are not limited to a single extended "rectangular" conformation with Lys side chains each at the same side of the molecule. Most probably, the RAFT molecule possesses a variety of low-energy conformers representing various orientation modes of the lysine side chains. Conformational equilibrium of many low-energy RAFT conformers is a more realistic view than suggestion of a single RAFT conformer existing in solution. These results are in good agreement with the available nmr data.

2. Conformational equilibrium in monocyclic analogues of RAFT obtained by replacements of conformationally flexible Gly residues for L-Ala, D-Ala, Aib, or D-Pro is not significantly shifted toward the target "rectangular" conformational type with four opposite Lys side chains at the same side of the molecule. However, one can select the desired type of β-reversals in the target conformers by the above replacements.

3. Introduction of disulfide bridges between positions 4 and 9 is a very powerful way to stabilize the target conformations of RAFT in the resulting bicyclic molecules by simple amino acid substitutions. Since these are easily accessible by current synthetic methods, the RAFT compounds designed in this study can be expected to be used widely as improved templates in the context of TASP assemblies with incorporated orthogonal peptide loops.

This work was supported in part by the NIH grant GM 48184 (GN) and by the Swiss National Science Foundation.

REFERENCES

1. Regan, L.; DeGrado, W. F. Science 1988, 241, 976–978.
2. DeGrado, W. F.; Wassermann, Z. R.; Lear, J. D. Science 1989, 243, 622–628.
3. Hecht, M. H.; Richardson, J. S.; Richardson, D. C.; Ogden, R. C. Science 1990, 249, 884–891.
4. Mutter, M.; Vuilleumier, S. Angew Chem (Engl) 1989, 28, 535–554.
5. Creighton, T. E. Proteins: Structures and Molecular Properties, 2nd ed.; Freemann, New York, 1993.
6. Mutter, M. Trends Biochem Sci 1988, 13, 261–265.
7. Mutter, M.; Tuchscherer, G. Makromol Chem Rapid Commun 1988, 9, 437–443.
8. Dumy, P.; Eggleston, I. M.; Esposito, G.; Nicula, S.; Mutter, M. Biopolymers 1996, 39, 297–308.
9. Dumy, P.; Eggleston, I. M.; Cervigni, S.; Sila, U.; Sun, X.; Mutter, M. Tetrahedron Lett 1995, 36, 1255–1258.
10. Anderson, S.; Anderson, H. L.; Sanders, J. K. M. Acc Chem Res 1993, 26, 469–475.
11. Tuchscherer, G.; Dörner, B.; Sila, U.; Kamber, B.; Mutter, M. Tetrahedron 1993, 49, 3559–3575.
12. Scheibler, L.; Dumy, P.; Stamou, D.; Duschl, C.; Vogel, H.; Mutter, M. Tetrahedron 1998, 54, 3725–3734.
13. Mutter, M.; Tuchscherer, G.; Miller, C.; Altmann, K.-H.; Carey, R. I.; Wyss, D. F.; Labhardt, A.; Rivier, J. E. J Am Chem Soc 1992, 114, 1463–1470.
14. Tuchscherer, G.; Servis, C.; Rivier, J.; Blum, U.; Corradin, G.; Mutter, M. Protein Sci 1992, 1, 1377–1386.
15. Mutter, M.; Dumy, P.; Garrouste, P.; Lehmann, C.; Mathieu, M.; Peggion, C.; Peluso, S.; Razaname, A.; Tuchscherer, G. Angew Chem (Engl) 1996, 35, 1481–1485.
16. Nikiforovich, G. V.; Prakash, O.; Gehrig, C. A.; Hruby, V. J. J Am Chem Soc 1993, 115, 3399–3406.
17. Nikiforovich, G. V. Int J Peptide Protein Res 1994, 44, 513–531.
18. Floegel, R.; Mutter, M. Biopolymers 1992, 32, 1283–1310.
19. Mierke, D. F.; Kurz, M.; Kessler, H. J Am Chem Soc 1994, 116, 1042–1049.
20. Gerber, P. R.; Müller, K. J Comput-Aided Mol Design 1995, 9, 251–268.
21. Gerber, P. R. J Comput-Aided Mol Design 1998, 12, 37–51.
22. Dunfield, L. G.; Burgess, A. W.; Scheraga, H. A. J Phys Chem 1978, 82, 2609–2616.
23. Nemethy, G.; Pottle, M. S.; Scheraga, H. A. J Phys Chem 1983, 87, 1883–1887.
24. Chalmers, D. K.; Marshall, G. R. J Am Chem Soc 1995, 117, 5927–5937.
25. Bosch, R.; Jung, G.; Schmitt, H.; Winter, W. Biopolymers 1985, 24, 979–999.
26. Zimmerman, S. S.; Scheraga, H. A. Biopolymers 1977, 16, 811–843.
27. Nikiforovich, G. V.; Hruby, V. J.; Prakash, O.; Gehrig, C. A. Biopolymers 1991, 31, 941–955.
28. Wüthrich, K. NMR of Proteins and Nucleic Acids; John Wiley: New York, 1986.
29. Hagler, A. T.; Huler, E.; Lifson, S. J Am Chem Soc 1974, 96, 5319–5327.
30. Schwyzer, R.; Ludescher, U. Helv Chim Acta 1969, 52, 2033–2040.
31. Llinas, M.; Klein, M. P. J Am Chem Soc 1975, 97, 4731–4737.
32. Wilmot, C. M.; Thornton, J. M. Protein Eng 1990, 3, 479–493.
33. Nikiforovich, G. V.; Vesterman, B.; Betins, J.; Podins, L. J Biomol Struct Dyn 1987, 4, 1119–1135.
34. Rose, G. D.; Gierasch, L. M.; Smith, J. A. Adv Protein Chem 1985, 37, 1–109.
35. Bean, J. W.; Kopple, K. D.; Peishoff, C. E. J Am Chem Soc 1992, 114, 5328–5334.
36. Karle, I. L.; Awasthi, S. K.; Balaram, P. Proc Natl Acad Sci USA 1996, 93, 8189–8193.
37. Haque, T. S.; Gellman, S. H. J Am Chem Soc 1997, 119, 2303–2304.
38. Späth, J.; Stuart, F.; Jiang, L.; Robinson, J. A. Helv Chim Acta 1998, 81, 1726–1738.
39. Tishchenko, G. N.; Andrianov, V. I.; Vainstein, B. K.; Woolfson, M. M.; Dodson, E. Acta Cryst Section D Biol Crystall 1997, 53 (part 2), 151–159.